PAPER

Effect of elevated substrate temperature deposition on the mechanical losses in tantala thin film coatings

To cite this article: G Vajente *et al* 2018 *Class. Quantum Grav.* **35** 075001

View the article online for updates and enhancements.

IOP ebooks™

Bringing together innovative digital publishing with leading authors from the global scientific community.

Start exploring the collection−download the first chapter of every title for free.

Effect of elevated substrate temperature deposition on the mechanical losses in tantala thin film coatings

G Vajente[1], **R Birney**[2,3], **A Ananyeva**[1], **S Angelova**[2,3], **R Asselin**[7], **B Baloukas**[4], **R Bassiri**[5], **G Billingsley**[1], **M M Fejer**[5], **D Gibson**[3], **L J Godbout**[7], **E Gustafson**[1], **A Heptonstall**[1], **J Hough**[8], **S MacFoy**[2,3], **A Markosyan**[5], **I W Martin**[8], **L Martinu**[4], **P G Murray**[8], **S Penn**[6], **S Roorda**[7], **S Rowan**[8], **F Schiettekatte**[7], **R Shink**[7], **C Torrie**[1], **D Vine**[3], **S Reid**[2,3] **and R X Adhikari**[1]

[1] LIGO Laboratory, California Institute of Technology, Pasadena, CA, United States of America

[2] SUPA, Department of Biomedical Engineering, University of Strathclyde, Glasgow, United Kingdom

[3] SUPA, Institute of Thin Films, Sensors and Imaging, University of the West of Scotland, Paisley, United Kingdom

[4] École Polytechnique de Montréal, Montréal, Quebec, Canada

[5] Stanford University, Stanford, CA, United States of America

[6] Hobart and William Smith Colleges, Geneva, NY, United States of America

[7] Université de Montréal, Montréal, Quebec, Canada

[8] SUPA, Institute for Gravitational Research, University of Glasgow, Glasgow, United Kingdom

E-mail: vajente@caltech.edu and ross.birney@strath.ac.uk

CrossMark

Abstract

Brownian thermal noise in dielectric multilayer coatings limits the sensitivity of current and future interferometric gravitational wave detectors. In this work we explore the possibility of improving the mechanical losses of tantala, often used as the high refractive index material, by depositing it on a substrate held at elevated temperature. Promising results have been previously obtained with this technique when applied to amorphous silicon. We show that depositing tantala on a hot substrate reduced the mechanical losses of the as-deposited coating, but subsequent thermal treatments had a larger impact, as they reduced the losses to levels previously reported in the literature. We also show that the reduction in mechanical loss correlates with increased medium range order in the atomic structure of the coatings using x-ray diffraction and Raman

spectroscopy. Finally, a discussion is included on our results, which shows that the elevated temperature deposition of pure tantala coatings does not appear to reduce mechanical loss in a similar way to that reported in the literature for amorphous silicon; and we suggest possible future research directions.

(Some figures may appear in colour only in the online journal)

1. Introduction

The recent detections of gravitational wave signals from the coalescence of black holes [1–4] and neutron stars [5] opened a new era in astronomy, and renewed the interest in the design and development of techniques to improve the sensitivity of the present generation of gravitational wave detectors such as Advanced LIGO [6], Advanced Virgo [7] and KAGRA [8].

The design sensitivity of Advanced LIGO is limited, in its most sensitive frequency range (20–300 Hz), by an equal contribution of quantum noise and thermal noise [6]. The dominant contribution to thermal noise is due to Brownian motion of the highly reflective, multilayer dielectric coatings deposited on the surfaces of the interferometer test masses [9]. Therefore, to further improve the sensitivity of the detectors in the present facilities, it is necessary to reduce the coating Brownian noise [10].

The Advanced LIGO high reflectivity multilayer coatings use alternating layers of silica (SiO_2) and titania-doped tantala (TiO_2–Ta_2O_5) [11, 12], where silica is the low refractive index material and titania-doped-tantala is the high refractive index material. The dominant contribution to the coating thermal noise comes from Brownian motion, which is directly related to the internal mechanical losses of the two materials [13–15]. In the state-of-the-art ion-beam-sputtered coatings used today, the measured mechanical loss angle for silica is 4×10^{-5} rad [12, 16], while for doped tantala it is 2.4×10^{-4} rad [11, 17]. Thus, the titania-doped-tantala layers are the dominant source of thermal noise.

There are many approaches under development to reduce the coating thermal noise: crystalline coatings [18], employing different materials and doping [19], or using different deposition and heat treatment techniques [20]. The goal for a medium term upgrade of Advanced LIGO [10] is to improve the sensitivity by a factor of about two. This corresponds to a reduction of mechanical loss in the coating by a factor of four. For coatings of the dimensions needed for the Advanced LIGO core optics, no single approach has, as of today, provided a viable method to reduce mechanical losses by this factor.

In this work we discuss the exploration of one promising technique to deposit low loss coatings, by heating the substrate during the deposition process. It has been known for some time that post-deposition annealing reduces mechanical losses [20]. Recently, experimental studies performed with amorphous silicon [21] showed a reduction of 2–3 orders of magnitude in the mechanical losses, by depositing the thin film on a substrate heated to about 85% of the glass transition temperature. Similar results were obtained with different deposition techniques and materials [22]. Keeping the substrate at an elevated temperature increases the mobility of the atoms deposited on the surface, which results in a more stable glass [23] and a reduced density of two-level tunnelling states [24, 25]; factors which have been shown to be correlated with mechanical losses in amorphous thin films. We should note here that post-deposition annealing at high temperature also allows an exploration of the energy landscape and a reduction of

the mechanical losses. However, both theoretical arguments and experimental results indicate that an elevated temperature during deposition allow a larger set of degrees of freedom to be explored by each atom that hits the surface, before being buried by the subsequent layers.

We focused our first experimental efforts on the study of thin films made of un-doped tantalum pentoxide (tantala). The lowest mechanical loss angle measured on thin films of this material after a post-deposition heat treatment is in the range 2.6×10^{-4} to 4.7×10^{-4} rad, depending on the deposition conditions [17, 26–30]. In this work we explored elevated temperature deposition using two different techniques that were readily available to us: magnetron sputtering and ion-beam sputtering [31].

Section 2 describes in detail both deposition techniques, as well as the substrates that were used. Section 3 describes the post-deposition heat treatment which was performed (annealing). Section 4 briefly describes the techniques used to measure the mechanical losses. Section 5 discusses the results of the measurements and section 7 describes the structural studies that were carried out to try to understand the evolution of the coatings' microscopic structure.

2. Deposition techniques

We deposited undoped tantalum pentoxide thin films using two different techniques and substrates.

2.1. Magnetron sputtering deposition

A first set of depositions consisted of 1 μm-thick layers of tantala, deposited using magnetron sputtering (MS) [31], on a fused silica disk (Corning 7980), 75 mm in diameter and 1 mm-thick. The depositions were carried out at the École Polytechnique de Montréal and the Université de Montréal. The surfaces of the disk were polished, while the edge of the disk was simply ground. It has been shown that mechanical losses in fused silica substrates are limited by the surfaces that are not polished [32]. The disks have two flat cuts on opposite sides, to break the degeneracy of the resonant modes. The measurable vibrational modes of the disks had frequencies between 1.1 kHz and 30 KHz. The substrates were heat treated for 9 h at 900 °C in air before deposition. This step ensures that all the substrates have an equivalent low mechanical loss angle, and that residual stresses due to the machining process are reduced [33].

A total of 12 disk samples were coated using magnetron sputtering: four at room temperature (in reality approximately 50 °C, due to the substrate heating up from the deposition process), and two disks at each of the following temperatures: 150 °C, 250 °C, 400 °C and 480 °C.

The magnetron-sputtered tantalum pentoxide films were deposited in a high vacuum CMS-18 process chamber built by Kurt J Lesker Co. Ltd, equipped with a 7.62 cm diameter tantalum target of 99.95% purity located ∼25 cm beneath the substrate holder. Prior to deposition, the base pressure was less than 10^{-7} Torr.

The 1 mm-thick fused-silica substrates were installed one at a time on a 15 cm-diameter rotating stainless steel holder, designed with a 7.62 cm-diameter hole in the middle, and supported at the edges by a 1 mm ledge. A 3 mm-thick Macor® puck of the same diameter as the substrate was placed on its backside and thus directly exposed to the halogen heating lamps positioned above the substrate holder. The high emissivity of Macor® (0.93 according to [34]) helped increase mid-infrared radiation in order to reach the highest temperature of 480 °C. The surface temperature of the substrates was pre-calibrated by installing a thermocouple

in direct contact with a substrate's surface before the deposition. The thermocouple was not installed during the actual deposition.

Each deposition run began by setting the desired temperature, increasing it at a rate of 5 °C min^{-1} and allowing it to stabilize for 30 min once reached. The sample was then subjected to a radio-frequency plasma cleaning procedure for 10 min in an Ar and O_2 gas mixture (2:1 Ar to O_2 ratio) at a pressure of 8 mTorr and a bias voltage between 90 and 100 V (the discharge power was maintained between 6 and 8 W). The tantalum target was then precleaned for 3 min in a pure Ar plasma at a discharge power of 440 W. Oxygen was then introduced into the chamber (60% O_2:Ar ratio at a pressure of 2 mTorr) and the discharge allowed to stabilize for 20 min to ensure steady-state conditions (bias cathode voltage of approximately −210 V). The main shutter was then opened and the film deposition started. It is important to note that the process itself typically heats the sample by 30 to 40 °C when depositing at room temperature; this temperature increase is expected to be smaller for samples heated to higher temperatures. The deposition time was kept constant for all samples and the deposition rate was seen to decrease from 2.27 Å s^{-1} to 2.07 Å s^{-1} as the temperature was increased. Following the deposition, the samples were cooled down to room temperature at a rate of 10 °C min^{-1}.

Rutherford backscattering spectrometry (RBS) confirms the expected stoichiometry of the films, and reveals the presence of Ar and H impurities at levels of 3% and 1.5% respectively. By combining RBS and ellipsometry measurements, we found the average density of the layers produced by MS to be $(7.5 \pm 0.3) \times 10^{22}$ atoms cm^{-3}. The combined uncertainty on the RBS and ellipsometry measurements did not allow us to find a correlation between the density and the loss angle or x-ray diffraction peak width (see also section 7). The refractive index of the tantala layer has also been measured. For all samples, except the one deposited at the highest temperature (480 °C), the refractive index is 2.14 ± 0.01. The sample deposited at 480 °C instead has a refractive index of 2.24 ± 0.01, however this sample showed signs of crystallization (see also section 7).

2.2. Ion beam sputtering deposition

A further set of depositions consisted of ∼0.5 μm-thick layers of tantala, deposited using ion beam sputtering (IBS) [31], on fused silica cantilevers. The depositions were carried out at SUPA, Institute of Thin Films, Sensors and Imaging, University of the West of Scotland. The samples were fabricated by dicing ∼150 μm-thick fused silica wafers (JGS1 material, 100 mm-diameter) into 45 mm-long strips, 5 mm-wide. These were then flame welded to a 3.1 mm-thick clamping block, of the same silica material, with area 10×10 mm^2, using a hydrogen-oxygen flame, on the 5 mm edge. The cantilevers were subsequently placed in boiling H_2O_2 (30 % w/w in H_2O) with 1 mol l^{-1} KOH dissolved, in order to clean the sample surface and to remove silica particulates associated with the welding process. Finally, the samples were annealed at 900 °C in air for 1 h. Further high temperature annealing did not change the substrate mechanical losses. The measurable vibrational modes of the cantilevers were between ∼300 Hz and ∼11 kHz.

A set of 5 cantilevers were coated by sputtering from a circular 4 inches diameter pure tantalum metal target of 0.125 inches thickness, purity 99.9% (Pi-Kem, UK), at room temperature and at elevated temperatures 100 °C, 200 °C, 300 °C and 400 °C. A further set of 6 cantilevers were then coated by sputtering from a 4 inches pure tantalum pentoxide target (Pi-Kem, UK), purity 99.99%, at room temperature and at elevated temperatures 100 °C, 200 °C, 300 °C, 400 °C and 500 °C (the maximum possible with the current setup). Additional JGS1 silica witness samples, of 20 mm diameter and 0.5 mm thickness, for optical and structural characterization, were coated in separate deposition runs using nominally identical conditions.
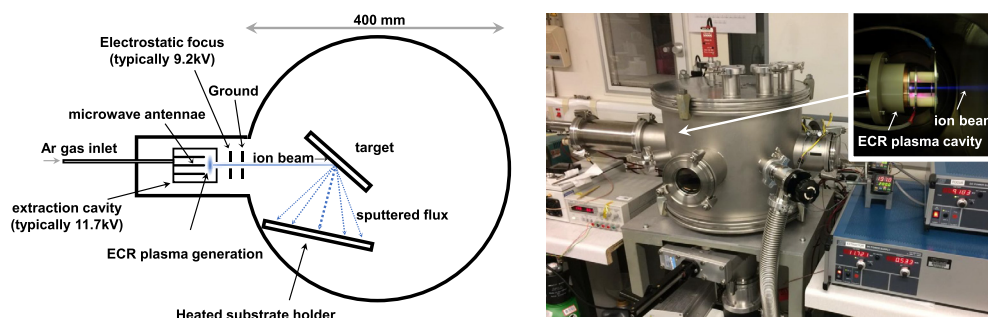
Figure 1. Schematic diagram (left) showing the configuration and geometry of the ion beam sputtering system, with images (right) of the chamber and ion source during operation (inset).

The IBS system was custom-built and uses a single electron cyclotron resonance (ECR) ion source developed by Polygon Physics [35], as shown in figure 1. The source uses a small $\lambda/4$ microwave (2.4 GHz) cavity, which is held at 11.7 kV in order to extract argon ions through a single aperture, which are focused into a near-parallel beam using electrostatic optics placed in front of the ECR cavity. The deposition system was specifically developed to be more flexible than standard RF ion beam sputtering, in addition to being potentially 'cleaner' due to the gridless extraction of the ions. However, the ion current is very low, typically in the range of $\sim 0.2 \rightarrow 0.5$ mA, which limits the deposition rate in this geometry to within a range of $1 \rightarrow 10$ Å min^{-1}. The base vacuum pressure was around 0.8×10^{-6} Torr or better prior to deposition, with the pressure rising to 6×10^{-5} Torr when injecting the required level of argon into the plasma cavity; finally increasing to 9×10^{-5} Torr once the reactive oxygen gas was fed into the chamber (introduced directly above the substrates being coated).

The temperature during deposition was monitored on the copper substrate holder, with calibration runs conducted by gluing PT100 resistance thermometers to silica cantilevers under identical conditions (the correction of the cantilever temperature with respect to the substrate holder was typically $20 \rightarrow 40$ °C, depending on deposition temperature). As with the magnetron coating process, the temperature was allowed to stabilize for a minimum of 30 mins before the deposition was commenced. The samples were allowed to cool naturally after deposition, with a maximum cooldown rate of 30 °C s^{-1} for the 500 °C deposition run, and slower cooldown rates for lower deposition temperatures.

3. Post-deposition heat treatments

After deposition, the mechanical losses of all samples were measured using the techniques described below in section 4. Additional structural measurements, described below in section 7, were also performed. Afterwards, a subset of the samples were subjected to a heat treatment cycle (annealing). In the case of the magnetron-sputtered samples, we first annealed them at 300 °C for 3 h, then at 400 °C for 3 h, and finally at 500 °C for 3 h, carrying out mechanical loss and structural measurements after each heat treatment cycle. In each case the samples were heated up at a rate of about 1 °C min^{-1}, and allowed to cool down at the same rate.

Similarly, the IBS samples were annealed for 5 h in air, at increasing temperatures of 100, 200, 300, 400, 500, 600 and 650 °C, and again allowed to cool naturally in the oven (maximum

Table 1. Material parameters used in finite element models.

	Silica	Tantala
Young's modulus (GPa)	73.2 [12]	140 [36]
Poisson ratio	0.164 [12]	0.28 [36]
Density (kg m^{-3})	2200 [12]	8200 [36]

ramp-up rate 4 °C s^{-1}, maximum ramp-down rate 3 °C s^{-1}. Mechanical loss measurements were performed after each annealing step.

The small difference in annealing time for the MS and IBS samples does not significantly affect the measured loss angle. Longer annealing times have been tested by the authors on a subset of the samples, and the measured loss angles found to be comparable.

4. Measurement of mechanical losses

The mechanical loss angle of each sample was measured by exciting its resonant modes and tracking the amplitude of the motion at the mode peak frequency over time. The ring-down time is directly linked to the total mechanical loss angle of the sample ϕ_{total}, including contributions from both the substrate losses and the coating layer losses:

$$A(t) = A(0)e^{-t\pi f \phi_{total}} \tag{1}$$

where f is the frequency of one of the resonant modes of the sample. To disentangle the two contributions, we built finite element models of the coated substrates. The models are based on the values for the Young's modulus, density and Poisson ratio of silica and tantala listed in table 1. The models are first tuned to accurately predict the resonant frequencies of the uncoated substrate. Afterwards, the coating thickness is tuned to the mean value over the whole surface measured by ellipsometry. Finally, the model can be used to extract the distribution of elastic energy in the substrate and in the coating. The ratio of the energy in the coating divided by the energy in the substrate is known as the dilution factor. It can be used to extract the coating loss angle from the total measured loss angle:

$$\phi_{total}^{(i)} = D^{(i)}\phi_{coating}^{(i)} + (1 - D^{(i)})\phi_{substrate}^{(i)} \tag{2}$$

where the subscript (i) refers to the vibrational modes, since the dilution factor differs from mode to mode. Also, in general, the loss angle may be frequency dependent. To accurately extract the coating loss angle, a measurement of the substrate loss is needed; this can be obtained by measuring the ring-down time of the uncoated sample, assuming that the deposition does not affect the substrate properties in a significant way. Typical numbers for the fused silica disks used in our experiments are $\phi_{substrate} \sim 10^{-7}$ and $\phi_{total} \sim 3 \times 10^{-6}$. The mechanical losses of the uncoated substrates used here are larger than what is expected for fused silica bulk [33], and they are limited by surface loss on the unpolished sides [32].

The coating loss angle could in principle be different for shear and bulk deformations [37]. Our finite element simulations show that most of the elastic energy is in shear. Moreover, recent results suggest that ϕ_{shear} and ϕ_{bulk} [38] are not significantly different. Therefore, in the analysis presented here we do not make this distinction. This approach also makes it simpler to compare our measurements with previous results reported in the literature, which also do not take into account the distinction between shear and bulk losses. Moreover, our main goal is to determine if there is any change in the mechanical loss that is deposition-process dependent, and therefore using a single loss angle is sufficient.

The samples coated by magnetron sputtering (75 mm-diameter disks) were measured at the LIGO Laboratory (Caltech) using a system based on the gentle nodal suspension [39, 40]. The fused silica substrate is supported at its center by a curved silicon surface, relying on gravity and friction between the sample and the support. This nodal suspension allows the measurements of all resonant modes between 1 kHz and 30 kHz with negligible clamping losses for all modes that have a node of non-motion at the center of the disk [41]. Four disks are mounted into one vacuum chamber, which allows the parallel measurement of four samples. The disks are excited using an electrostatic comb drive [42], and the motion is read-out with an optical lever system; a HeNe laser beam is reflected off the disk surface, close to the edge, and the beam displacement is measured with a quadrant photo-detector (QPD). The output signals are sampled at 65 kHz and saved to disk to be processed offline. This excitation and data acquisition system allows the simultaneous measurement of the ring downs of all resonant modes of the four samples. More details on the measurement system can be found in [40].

In the case of the coatings deposited on cantilevers by IBS, each sample was measured before and after coating using a readout technique similar to the one described above, but with a few notable differences. The silica cantilevers were each secured inside a vacuum chamber by fixing the clamping block in place with a stainless steel clamp. A He–Ne laser outside the chamber was then directed through a chamber window, incident upon the edge of the cantilever, and passed through a second window onto a split photodiode detector, again outside the chamber. The cantilever creates a shadow on the laser spot, the displacement of which (due to excitation of the cantilever) is then measured; each mode was measured and recorded individually by an automated LabView program for offline analysis. The mechanical losses were then calculated in the same way as with the disk samples, using equation (2), with dilution factors obtained from finite element models of the cantilever geometry.

5. Results

The coating loss angle measured for all 12 MS samples is shown in figure 2. For each sample, several resonant modes could be measured, with frequencies between 1 kHz and 20 kHz. All samples were measured after deposition, and before any additional treatment. Then, 5 samples (two deposited at room temperature and one for each of the other deposition temperatures) were treated with annealing cycles, at increasing temperatures of 300, 400 and 500 °C. The results of all mechanical loss measurements, for all the frequencies, are shown in figure 2.

For the majority of samples, the dependence of the loss angle upon the mode frequency is rather weak and, in most cases, a clear trend is difficult to identify. For these reasons, and to facilitate easier comparison between samples, the loss angle has been averaged over frequency for each sample; the results are shown in figure 3. One can first observe that there is a reduction of mechanical losses in the as-deposited samples, when the substrate is at an elevated temperature during deposition. However, the measured losses further improved with post-deposition annealing, reaching a level as low as 4.5×10^{-4} rad; comparable with what is reported in the literature for annealed pure tantala [27, 29, 30].

For the IBS coatings, figure 4 shows the measured loss angles for all resonant modes and all samples. Again, the dependence of loss angle upon mode frequency is quite weak in most cases; therefore, the loss angles were again averaged over all resonant frequencies for ease of comparison between different samples (see figure 5). The IBS coatings showed broadly similar results to the magnetron sputtered coatings, in that mechanical loss is reduced by elevated temperature deposition. However, the measured losses further improved with post-deposition
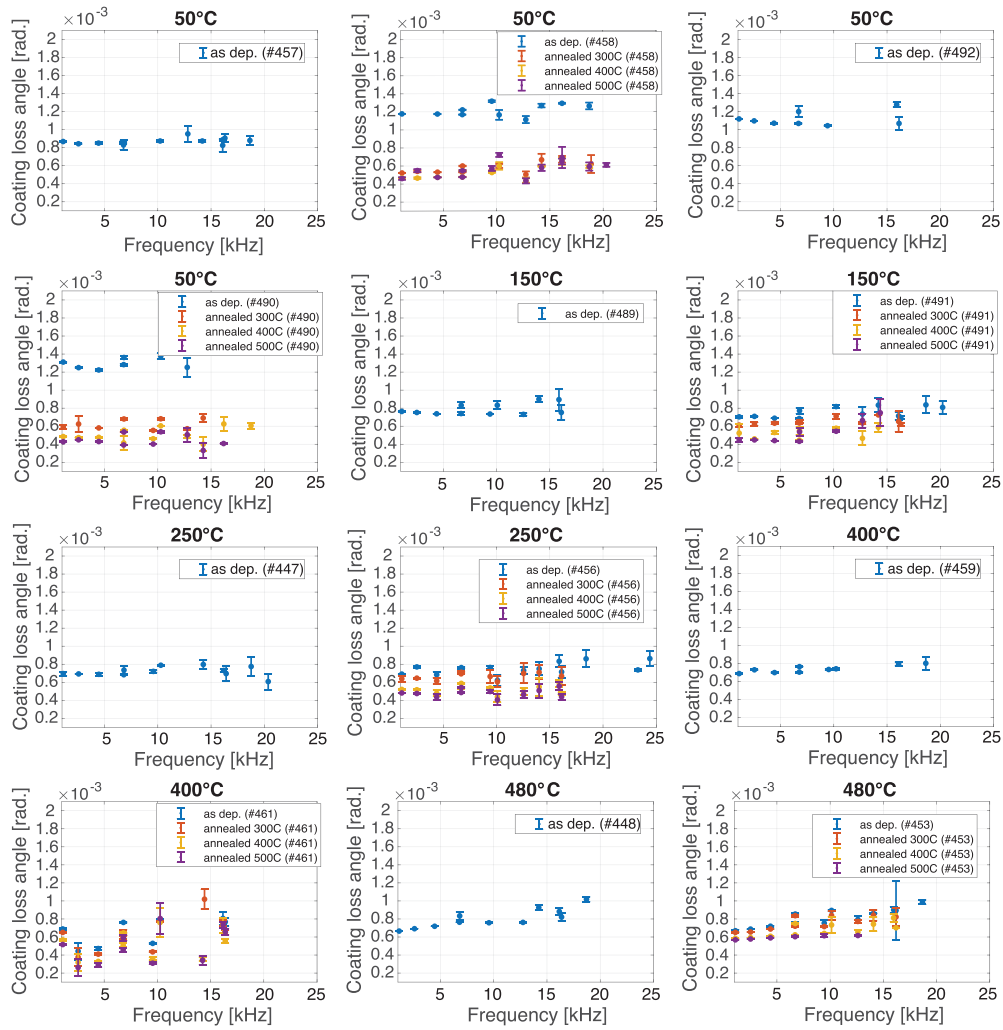
Figure 2. Summary of all measurements performed on the magnetron sputtered samples. Each panel corresponds to a different sample. The title shows the temperature at which the coating was deposited, while the different traces (if present) in each panel refer to the coating as-deposited or after subsequent annealing treatments. The numbers in the legend are unique identification numbers for each substrate. The error bars at each frequency are 95% confidence intervals computed from the standard deviation of repeated measurements.

annealing, with the average loss reaching $2.7 \pm 0.8 \times 10^{-4}$ rad, which is in line with the lower end of previously reported measurements [26], and also close to the loss angle measured on the titania-doped-tantala used in the Advanced LIGO coatings [17]. It should be noted that there are two significant differences between the ECR ion beam sputtering process employed in this work and current industry standard processes: a significantly slower deposition rate and a higher extraction potential. Further investigations of these factors, in relation to the achievable levels of mechanical loss, are therefore worth exploring.

In summary, the mechanical loss of as-deposited tantala improves with the deposition temperature up to about 250 °C and then remains roughly constant, although at a value lower
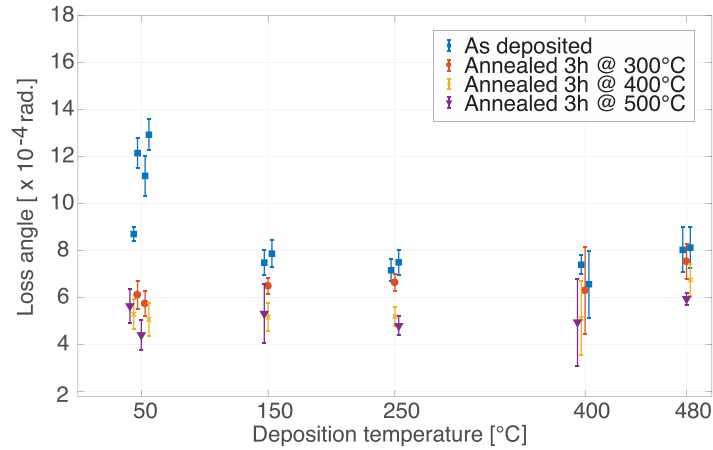
Figure 3. Averaged mechanical loss angle for magnetron sputtered tantala. The values shown here are obtained by averaging the results shown in figure 2, over all frequencies. The error bars are 95% confidence intervals computed from the standard deviation of the loss angles measured for the different modes for each sample (the uncertainty in the single frequency measurements are negligible). A random horizontal shift of the points have been added to improve the readability of the plot.

than that measured on room-temperature-deposited samples. However, high temperature annealing erases the deposition history of the coating. The main remaining difference is the fact that coatings deposited by IBS have about 1.6 times lower mechanical loss angle than the coatings deposited by MS. It is worth noting that a small discrepancy has been observed in the past between mechanical loss measurements performed on disk with gentle nodal suspension systems and cantilevers. However, as shown in [12], the mechanical loss measured on disks were lower than the mechanical losses measured on cantilever. Therefore we believe that the larger difference in our samples is due to the deposition techniques.

6. Structural characterization: measurement techniques

6.1. X-ray diffraction

X-ray diffraction study of all MS samples was carried out on a PANalytical X'Pert PRO x-ray diffraction system in parallel beam mode at the Stanford Nano Shared Facilities. For these measurements, in order to obtain maximum scattered intensity from the deposited thin films, while minimizing the contribution from the substrate, the incident x-ray beam angle was fixed at 1.5° while the detector was scanned from 10° to 90°. The angle of divergence for the incident and diffracted beams was 0.04° and 0.27°, respectively. For polycrystalline samples, such a scan results in the same Bragg peaks as a standard $\theta - 2\theta$ scan but with slightly different relative peak intensities. In amorphous thin films, one would not observe sharp Bragg peaks but broad diffraction peaks. Once properly reduced (i.e. expressed as oscillations about the structure factor versus scattering vector) a Fourier transform of these broad structures gives the atomic radial distribution function (see, e.g. [43]). Therefore, increased medium range order in the atomic structure of an amorphous material usually results in sharper (less broad) diffraction features.
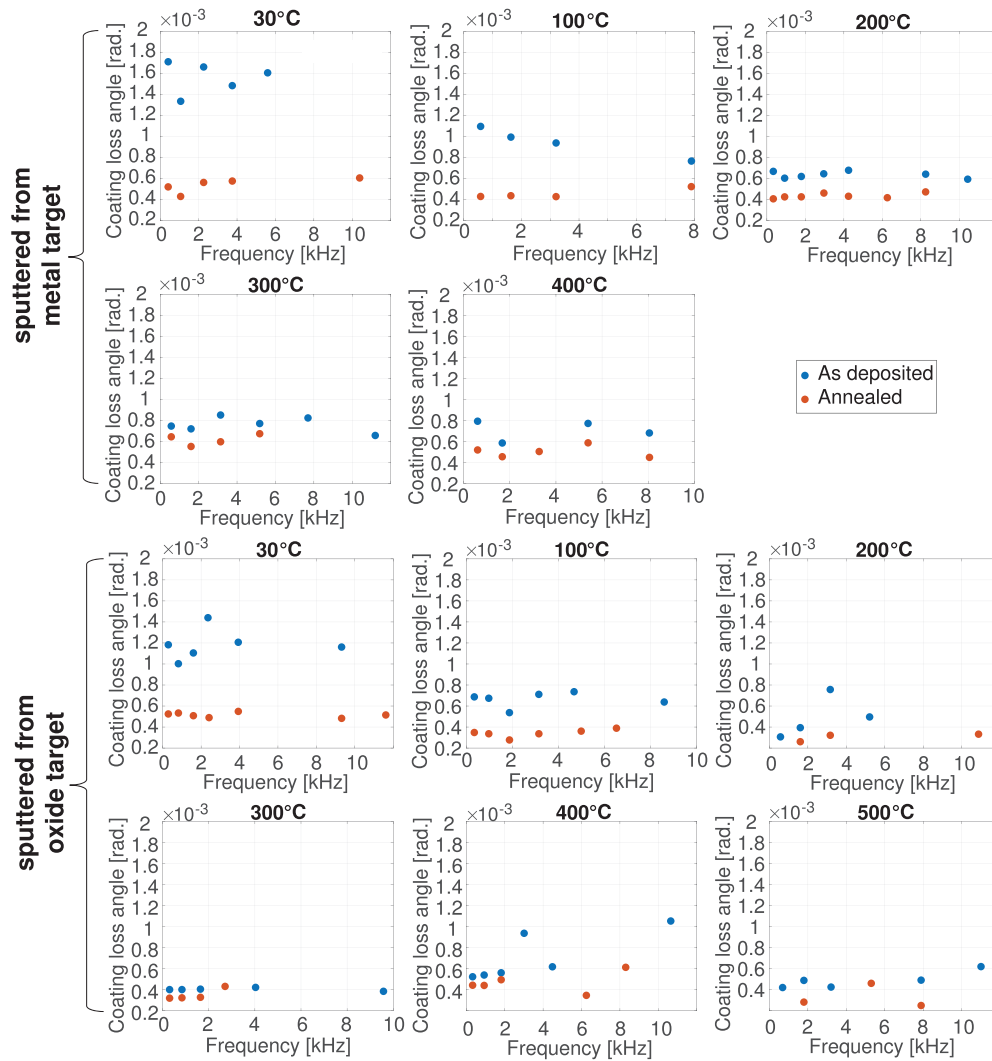
Figure 4. Summary of all the measurements performed on ion beam sputtered samples. Each panel corresponds to a different sample. The title shows the temperature at which the coating was deposited, with separate traces to show the mechanical loss as-deposited and post annealing treatment (all at 600 °C for 1 h). The uncertainty for all data points is about 1%, and not visible in the plot.

6.2. Raman spectroscopy

Raman spectroscopy was performed using a Renishaw Invia Reflex Raman microscope employing an Argon laser operating at 514 nm, non-polarized in a backscattering geometry. The 25.0 mW laser beam was focused to a circular spot of 2 μm diameter. Rayleigh scattering was removed by an edge filter with a 90 cm^{-1} cut-off. A 1800 l mm^{-1} grating spectrometer dispersed the scattered light onto 1040 × 256 pixel CCD resulting in a spectral resolution of 1.0 cm^{-1}. Three measurements were carried out at different locations on each sample, and the average is plotted in figure 8. Individual measurements were also analyzed to check for non-uniformity; no obvious effect was found. The Raman spectrum of an amorphous material
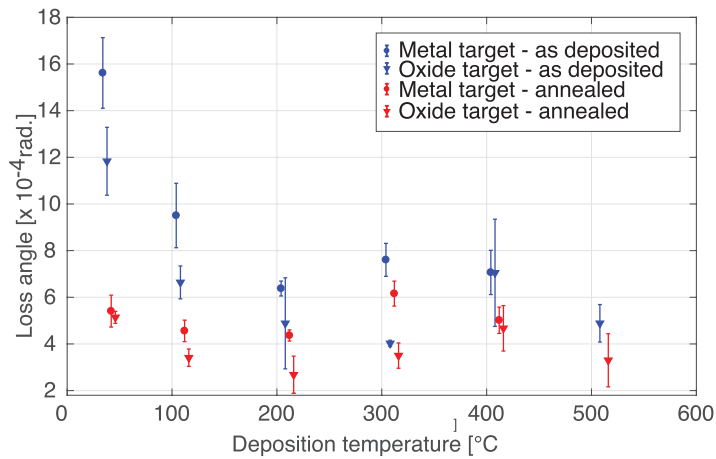
Figure 5. Averaged mechanical loss angle for ion beam sputtered tantala. The values shown here are obtained by averaging the results shown in figure 4 over all frequencies. The error bars show the standard error associated with the spread in the measured mechanical losses. The slight change in deposition temperature between the metal and oxide target sputtered coatings are associated with improvements in the calibration of the temperature readout carried out between these sets of coating runs.

resembles its vibrational density of states, since the selection rules that affect the Raman scattering in crystalline materials are not operative. The shape of the Raman spectrum can be described in an ad-hoc fashion, as a combination of Lorentzian curves each representing one band in the (crystalline) phonon dispersion diagram or from a molecular dynamics simulation of the material. For the case of Ta_2O_5, the first approach requires 19 Lorentzians [44]; the vibrational density of states deduced from molecular dynamics was reported by [45].

7. Structural studies: results

Several structural studies (x-ray diffraction (XRD) and Raman spectroscopy) were carried out to gain more insights into the effect of deposition temperature and annealing, and to look for residual differences between coatings deposited at different substrate temperatures.

7.1. X-ray diffraction

As a first step, XRD measurements were performed for all samples to check for possible crystallization, both immediately after deposition and after subsequent heat treatment cycles. Figure 6 shows the resulting diffraction patterns for the IBS samples and the MS samples. In the case of IBS samples, XRD scans were performed on the samples as deposited, and after the last annealing step at 600 °C. No crystallization was detected for any deposition temperature in IBS samples, while the MS coating deposited on a substrate at 480 °C showed clear signs of crystallization. Crystallization in MS thin films has previously been observed at deposition temperatures above 450 °C [46, 47]. No further crystallization was induced by the post-deposition annealing cycles. The IBS deposition is likely to produce a denser coating, thus suppressing crystallization; other workers have also reported crystallisation temperature of amorphous thin films to increase with increasing packing density [48].
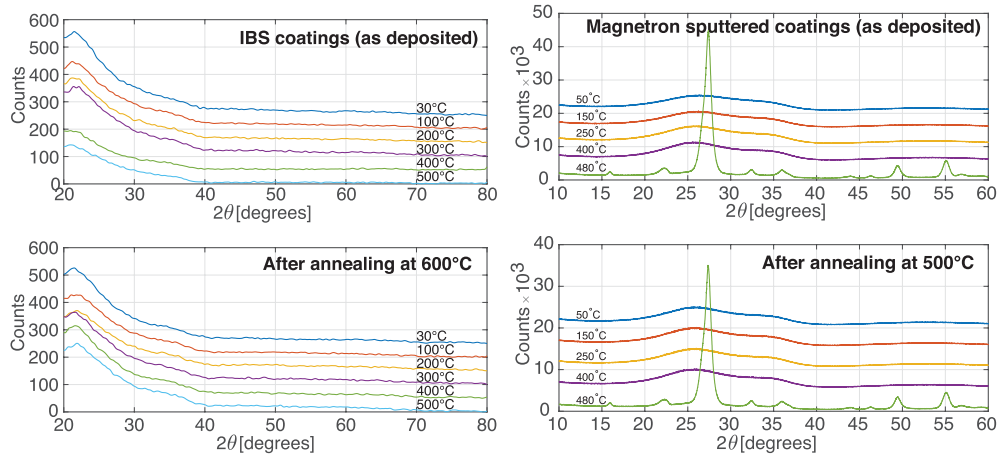
Figure 6. Left. XRD diffraction patterns for ion beam deposited tantalum pentoxide films, sputtered from an oxide target, before (top) and after (bottom) annealing at 600°C. The temperatures listed in the graph correspond to the different substrate temperature during deposition. XRD scans were carried out using a Siemens D5000 x-ray diffractometer at room temperature with Cu K_α radiation ($\lambda = 0.154$ nm) in the range of 2θ between 20° and 80° (2 s per scan, step size $= 0.02°$). Right. X-ray diffraction curves for a selection of the magnetron sputtered samples, before (top) and after (bottom) annealing. In each panel, the curves corresponding to different deposition temperatures have been shifted vertically by an arbitrary amount for readability.

7.2. Medium range order and loss angle

XRD measurements were also used to characterize more subtle changes in the microscopic structure of the coatings. In particular, medium range order (the local atomic structure in the range of 0.5–5 nm) in amorphous covalent glasses can be characterized by the *first sharp diffraction peak* (FSDP) in the XRD spectrum [49]. Both the position and width of the FSDP provide information on the statistical distribution of bond angles [50]. We have therefore attempted to correlate the loss angle measurements with the width and position of the FSDP on the MS samples. Since in Ta_2O_5 the FSDP is very asymmetric with a large shoulder on the high-angle side, we selected an angular range of 2θ between 16 and 28° and fit the data with a Gaussian peak plus a constant offset. Figure 7 shows the results for the as-deposited and post-annealing MS coatings. The width of the FSDP is correlated with the deposition temperature, as visible in the left panel of figure 7: for both the as-deposited samples and the annealed samples, the peak width decreases with increasing deposition temperature. The effect of annealing is also important: annealed samples show narrower peaks with respect to the corresponding as-deposited sample.

The correlation between the loss-angle measurements and the FSDP-peak widths is shown in the right panel of figure 7. The anneal temperature in all cases was 500 °C. Very similar results are obtained when comparing the loss angle measurements to the FSDP position instead of width (not shown here). There is a weak linear correlation (correlation coefficient $r = 0.78$) between the FSDP width and the mechanical loss angle: lower loss angles correspond to narrower peaks.

In view of the good linear fit for most data points, we can speculate that a narrower FSDP, corresponding to an increased medium range order, is correlated to lower loss angle. However, for two samples (as deposited, 250 °C and 400 °C), another mechanism inhibited low loss
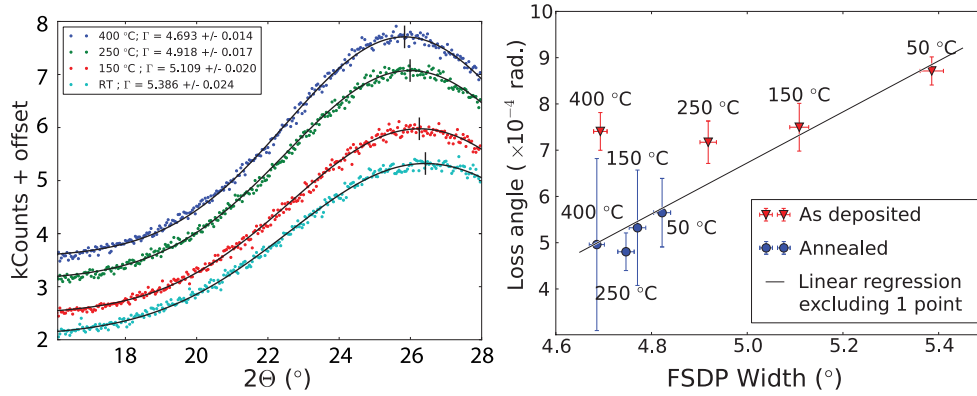
Figure 7. Left. First sharp diffraction peak (small angle side only) of four magnetron sputtered samples, before annealing. Spectra have been offset vertically for clarity. From top to bottom : deposited at 400 °C, 250 °C, 150 °C, and at room temperature. The solid lines show a Gaussian fit to the experimental data. The peak positions determined by the fit are shown as vertical lines across the maximum of each curve, and the peak widths are reported in the legend. The quoted uncertainty corresponds to the 1-sigma increase in chi-squared as determined by the fitting routine. Right. Mechanical loss angle as a function of the FSDP width for magnetron sputtered samples, before (red triangles) and after (blue circles) annealing at 500 °C . The solid line is a linear fit to all datapoints, excluding the one deposited at 400 °C before annealing.

angles in spite of good medium range order. This could be caused by, for example, a strain mismatch between substrate and deposited layer, or some other issue that can be remedied with the post-deposition anneal. Still, aiming at low loss angles one should strive for increased medium range order [51]. This suggests that the deposition should be carried out at as high a deposition temperature as possible, and post-deposition annealing should be carried out at as high a temperature as possible. Indeed, in the case of pure amorphous silicon, high medium range order, as characterized by x-ray diffraction and Raman spectroscopy, was obtained by a short, high temperature flash anneal [52]; crystallization was avoided by limiting the anneal time to a few seconds. It is therefore worthwhile to investigate the loss angle in samples deposited at temperatures above 400 °C (but below 480 °C which results in partly crystalline MS films) and subsequently heat treatment at higher anneal temperatures, perhaps using rapid thermal annealing.

7.3. Raman spectroscopy and loss angle

Raman spectroscopy is a powerful tool to detect structural relaxation, as shown in amorphous silicon in [53]. This type of structural relaxation, or change in the medium range ordering, involves a thermally activated atomic rearrangement of the otherwise static atomic structure. Based on our XRD observations, we surmise that the dynamical relaxation or internal friction mechanisms which we are trying to minimize in the Ta_2O_5 layers are reduced in materials that have undergone such a structural relaxation of the permanent atomic structure. In other words, the mechanical loss angle in Ta_2O_5 may be correlated to medium range order, and in turn the medium range order in amorphous Ta_2O_5 can perhaps be detected by Raman spectroscopy. Therefore we decided to measure the Raman spectrum of all the samples for which the mechanical loss angle had also been measured. The Raman spectrum of Ta_2O_5 is much more complicated than that of amorphous silicon: in the case of silicon, there are only four

main bands (TO-, TA-, LA-, LO -like) relatively well separated, so that one can determine the width, position, and relative intensity of each band. In particular, the width of the amorphous silicon TO-like band has been shown to depend on the average distortion of the tetrahedral bond angle, and hence to be a good indicator of medium range order [54]. In the case of Ta_2O_5, the Raman spectra of the crystalline and amorphous phases can be described with a fit containing essentially 19 Lorentzian curves [44], and most of those are overlapping. This makes it difficult to reliably extract the width of any single band from the Ta_2O_5 Raman spectrum.

The left panel in figure 8 shows the Raman spectrum measured for each of the magnetron sputtered samples, after annealing. The main feature in all spectra is a large peak centered near $700\,cm^{-1}$, which is due to at least 4 separate bands according to the fit described in [44]. Molecular dynamics [45] indicate this frequency range corresponds to bending and stretching movements involving 3 Ta coordinated oxygen atoms. One spectrum (deposition temperature $= 480\,°C$) also shows a peak near $200\,cm^{-1}$ indicative of crystallization [44], as already noted in the XRD analysis (see figure 6). The right panel in figure 8 compares the mechanical loss angles of all samples with the Raman peak width. As can be observed, this analysis is inconclusive: lower mechanical losses are weakly correlated to narrower peaks (correlation coefficient $r = 0.71$), similarly to what was already determined in the XRD analysis. We have extracted many more parameters from the Raman spectra, such as the relative intensity of the bands at 90 and $650\,cm^{-1}$ or the mean position rather than FWHM of the main peak, and evaluated their behavior versus the loss angle or anneal temperature. So far, no parameter measured by Raman spectroscopy shows a clear correlation with the mechanical loss angle even though in all samples the anneal treatment leads to both a decrease in Raman peak width and mechanical loss angle. Further efforts are needed, especially from a simulation point of view, in order to interpret the features of these spectra.

8. Discussion of the results

In this work, we explored the effect of deposition on a substrate held at elevated temperature on the mechanical loss of pure tantala. The results obtained from two different deposition techniques agree quite well: depositing the coating on a hot substrate improves the mechanical loss. However, the as-deposited coatings did not show a significant improvement of mechanical loss with respect to previous results for room-temperature-deposited films after optimal post-deposition annealing. Additionally, heat treatment after deposition appears to have a much larger effect than elevated temperature deposition: after annealing at about $400\,°C$ all coatings, regardless of the deposition technique or the substrate temperature, show mechanical loss in the range $2.7-4 \times 10^{-4}$ rad, in line with previous results. It is worth noting that post annealing the IBS films exhibit about 1.6 times lower loss angle than the MS films: further investigations are needed to confirm if this difference is due to the deposition technique, or because the IBS coatings were deposited at a significantly lower rate.

Structural studies were carried out to correlate the mechanical loss with increased medium range order. Lower mechanical losses are correlated with a narrower width of the first diffraction peak in x-ray measurements and, more weakly, with the width of the main Raman spectrum peak. Although the substrate temperature during deposition played a role in determining the peak widths as well as the mechanical loss, the effect of post-deposition heat treatment is much more significant: annealed samples systematically showed lower loss angles and more relaxed structure (narrower peaks).

In conclusion, we could not achieve for tantala the same level of reduction in mechanical loss angle observed in amorphous silicon [21]. From a theoretical point of view, mechanical
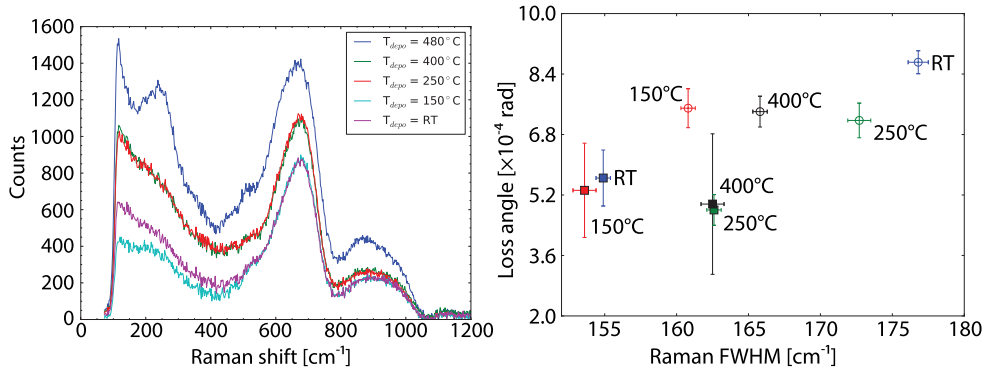
Figure 8. Left. Raman spectra of five magnetron sputtered samples, after annealing. From top to bottom: deposited at 480 °C, 400 °C nearly overlapping with the one deposited at 250 °C, 150 °C, and at room temperature. Right. Loss angle as a function of the full width at half maximum (FWHM) of the main peak of the Raman spectrum, for the magnetron sputtered samples. Open circles correspond to measurements performed on samples as-deposited, while solid squares to measurements performed on samples annealed at 500 °C. The substrate temperature during deposition is written next to each data point.

losses are associated with low-energy excitations usually modeled as two-level systems (TLS). The structure of the energy landscape in glasses depends on the fabrication history: a detectable change in the glass structure is expected to happen when the deposition is carried out at a significant fraction (85%) of the glass transition temperature [24, 25]. This was indeed observed in amorphous silicon. If, as expected from experiments and models, the fraction of the glass transition temperature at which the density of TLS reduces is universal, we might expect any effect to be visible in tantala for temperatures much higher than those explored in this study, which was limited by the incipient crystallization of the thin film. It is possible that the glass transition temperature of tantala is too high to be practically reachable before crystallization of the coating is induced. A strategy that will be explored in the future is the prevention of crystallization, either geometrically, with nano-layers [55], or chemically, with the addition of dopants to tantala, for example titania [11] or zirconia [17].

Further investigations are needed to better understand the microscopic structure of tantala coatings. Future planned experiments will use x-ray scattering [56] and electron diffraction [57], combined with atomic deposition modeling [58], to perform a detailed analysis of the medium range order. Such studies could elucidate the atomic structure patterns that play a significant role in the mechanical loss, in particular with elevated temperature deposition and post-deposition heat treatment of tantala and other oxides.

The results reported here indicate that elevated temperature deposition of pure tantala might not be a viable solution for low mechanical loss coatings for future gravitational wave detectors. We do not have enough data to generalize these results to other materials, or to doped tantala. Future investigations will therefore focus on doping, other oxides with lower melting temperatures, and alternative deposition techniques, such as ion-beam-assisted IBS and lower deposition rates.

Acknowledgments

ORCID iDs

G Vajente ⬤ https://orcid.org/0000-0002-7656-6882
R Birney ⬤ https://orcid.org/0000-0002-4766-0757

References

[1] Abbott B P *et al* 2016 Observation of gravitational waves from a binary black hole merger *Phys. Rev. Lett.* **116** 061102
[2] Abbott B P *et al* 2016 GW151226: observation of gravitational waves from a 22-solar-mass binary black hole coalescence *Phys. Rev. Lett.* **116** 241103
[3] Abbott B P *et al* 2017 GW170104: observation of a 50-solar-mass binary black hole coalescence at redshift 0.2 *Phys. Rev. Lett.* **118** 221101
[4] Abbott B P *et al* 2017 GW170814: a three-detector observation of gravitational waves from a binary black hole coalescence *Phys. Rev. Lett.* **119** 141101
[5] Abbott B P *et al* 2017 GW170817: observation of gravitational waves from a binary neutron star inspiral *Phys. Rev. Lett.* **119** 161101
[6] Abbott B P *et al* 2016 The advanced LIGO detectors in the era of first discoveries *Phys. Rev. Lett.* **116** 131103
[7] Acernese F *et al* 2015 Advanced virgo: a second-generation interferometric gravitational wave detector *Class. Quantum Grav.* **32** 024001
[8] Akutsu T *et al* 2015 Large-scale cryogenic gravitational-wave telescope in japan: KAGRA *J. Phys.: Conf. Ser.* **610** 012016
[9] Harry G M *et al* 2002 Thermal noise in interferometric gravitational wave detectors due to dielectric optical coatings *Class. Quantum Grav.* **19** 897
[10] Miller J *et al* 2015 Prospects for doubling the range of Advanced LIGO *Phys. Rev.* D **91** 062005
[11] Harry G M *et al* 2007 Titania-doped tantala/silica coatings for gravitational-wave detectors *Class. Quantum Grav.* **24** 405
[12] Granata M *et al* 2017 Mechanical loss in state-of-the-art amorphous optical coatings *Phys. Rev.* D **93** 012007

[13] Liu Y T and Thorne K S 2000 Thermoelastic noise and homogeneous thermal noise in finite sized gravitational-wave test masses *Phys. Rev.* D **62** 122002

[14] Levin Y 1998 Internal thermal noise in the LIGO test masses: a direct approach *Phys. Rev.* D **57** 659

[15] Levin Y 2008 Fluctuation-dissipation theorem for thermo-refractive noise *Phys. Lett.* A **372** 1941

[16] Penn S D *et al* 2003 Mechanical loss in tantala/silica dielectric mirror coatings *Class. Quantum Grav.* **20** 2917

[17] Flaminio R *et al* 2010 A study of coating mechanical and optical losses in view of reducing mirror thermal noise in gravitational wave detectors *Class. Quantum Grav.* **27** 084030

[18] Cole G D *et al* 2016 High-performance near- and mid-infrared crystalline coatings *Optica* **3** 647

[19] Reid S *et al* 2016 Development of mirror coatings for gravitational wave detectors *Coatings* **6** 61

[20] Martin I W *et al* 2010 Effect of heat treatment on mechanical dissipation in Ta_2O_5 coatings *Class. Quantum Grav.* **27** 225020

[21] Liu X *et al* 2014 Hydrogen-free amorphous silicon with no tunneling states *Phys. Rev. Lett.* **113** 025503

[22] Pérez-Castañeda T *et al* 2014 Suppression of tunneling two-level systems in ultrastable glasses of indomethacin *Proc. Natl Acad. Sci.* **111** 11275

[23] Berthier L and Ediger M D 2016 Facets of glass physics *Phys. Today* **69** 40

[24] Phillips W A 1972 Tunneling states in amorphous solids *J. Low Temp. Phys.* **7** 351

[25] Leggett A J and Vural D C 2013 Tunneling two-level systems model of the low-temperature properties of glasses: are smoking gun tests possible? *J. Phys. Chem.* B **117** 12966

[26] Martin I W *et al* 2009 Comparison of the temperature dependence of the mechanical dissipation in thin films of Ta_2O_5 and Ta_2O_5 doped with TiO_2 *Class. Quantum Grav.* **26** 155012

[27] Crooks D R M *et al* 2006 Experimental measurements of mechanical dissipation associated with dielectric coatings formed using SiO_2, Ta_2O_5 and Al_2O_3 *Class. Quantum Grav.* **23** 4953

[28] Cesarini E *et al* 2011 Silica as a key material for advanced gravitational wave detectors *J. Non-Cryst. Solids* **357** 2005

[29] Li T *et al* 2014 Measurements of mechanical thermal noise and energy dissipation in optical dielectric coatings *Phys. Rev.* D **89** 092004

[30] Principe M *et al* 2015 Material loss angles from direct measurements of broadband thermal noise *Phys. Rev.* D **91** 022005

[31] Vossen J L 1978 *Thin Film Processes* (Amsterdam: Elsevier)

[32] Cagnoli G *et al* 2017 Mode-dependent mechanical losses in disc resonators *Phys. Lett.* A (https://doi.org/10.1016/j.physleta.2017.05.065) in press

[33] Penn S *et al* 2006 Frequency and surface dependence of the mechanical loss in fused silica *Phys. Lett.* A **352** 3

[34] Carlomagno G M and Cardone G 2010 Infrared thermography for convective heat transfer measurements *Exp. Fluids* **49** 1187

[35] Polygon Physics ECR source (https://www.polygonphysics.com/, accessed 16/02/18)

[36] Çetinörgü E *et al* 2009 Mechanical and thermoelastic characteristics of optical thin films deposited by dual ion beam sputtering *Appl. Opt.* **48** 4536

[37] Hong T, Yang H, Gustafson E, Adhikari R and Chen Y 2013 Brownian thermal noise in multilayer coated mirrors *Phys. Rev.* D **87** 082001

[38] Abernathy M *et al* 2017 Bulk and shear mechanical loss of titania-doped tantala *Phys. Lett.* A (https://doi.org/10.1016/j.physleta.2017.08.007) in press

[39] Cesarini E *et al* 2009 A gentle nodal suspension for measurements of the acoustic attenuation in materials *Rev. Sci. Instrum.* **80** 053904

[40] Vajente G *et al* 2017 A high throughput instrument to measure mechanical losses in thin film coatings *Rev. Sci. Instrum.* **88** 073901

[41] Granata M *et al* 2015 Internal friction and young's modulus measurements on SiO_2 and Ta_2O_5 films done with an ultra-high Q silicon-wafer suspension *Arch. Metall. Mater.* **60** 365–70

[42] Cadez A *et al* 1988 Measuring high mechanical quality factors of bodies made of bare insulating materials *J. Phys. E: Sci. Instrum.* **21** 453

[43] Elliott S R 1983 *Physics of Amorphous Materials* (New York: Longman)

[44] Joseph C, Bourson P and Fontana M 2012 Amorphous to crystalline transformation in Ta_2O_5 studied by raman spectroscopy *J. Raman Spectrosc.* **43** 1146–50

[45] Damart T *et al* 2016 Numerical study of the structural and vibrational properties of amorphous Ta$_2$o$_5$ and TiO$_2$-doped Ta$_2$O$_5$ *J. Appl. Phys.* **119** 175106

[46] Nakagawa Y, Gomi Y and Okada T 1987 Deposition of new piezoelectric Ta$_2$O$_5$ thin films and their surface acoustic-wave properties *J. Applied Phys.* **61** 5012

[47] Guoping C, Lingzhen L, Suixin Z and Haokang Z 1990 Structures and properties of a Ta$_2$O$_5$ thin film deposited by dc magnetron reactive sputtering in a pure O$_2$ atmosphere *Vacuum* **41** 1204–6 (*Selected Proc. 11th Int. Vacuum Congress (IVC-11), 7th Int. Conf. on Solid Surfaces (ICSS-7)*)

[48] Chen H-C, Lee K-S and Lee C-C 2008 Annealing dependence of residual stress and optical properties of TiO$_2$ thin film deposited by different deposition methods *Appl. Opt.* **47** C284–7

[49] Elliot S 1991 Origin of the first sharp diffraction peak in the structure factor of covalent glasses *Phys. Rev. Lett.* **67** 711

[50] Lucovsky G and Phillips J 2010 Nano-regime length scales extracted from the first sharp diffraction peak in non-crystalline SiO$_2$ and related materials: device applications *Nanoscale Res. Lett.* **5** 550

[51] Bassiri R *et al* 2013 Correlations between the mechanical loss and atomic structure of amorphous TiO$_2$-doped Ta$_2$O$_5$ coatings *Acta Mater.* **61** 1070

[52] de Wit L, Roorda S, Sinke W, Saris F, Berntsen A and van der Weg W 1992 Structural relaxation of amorphous Si induced by high temperature annealing *Mater. Res. Soc. Symp. Proc.* 205 3

[53] Tsu R, Gonzalez-Hernandez J and Pollack F 1984 Determination of energy barrier for structural relaxation in a-Si and a-Ge by Raman scattering *J. Non-Cryst. Solids* **66** 109

[54] Beeman D, Tsu R and Thorpe M 1985 Structural information from the Raman spectrum of amorphous silicon *Phys. Rev.* B **32** 874

[55] Pan H-W *et al* 2014 Thickness-dependent crystallization on thermal anneal for titania/silica nm-layer composites deposited by ion beam sputter method *Opt. Express* **22** 29847

[56] Shyam B *et al* 2016 Measurement and modeling of short and medium range order in amorphous Ta$_2$O$_5$ thin films *Sci. Rep.* **6** 32170

[57] Hart M J *et al* 2016 Medium range structural order in amorphous tantala spatially resolved with changes to atomic structure by thermal annealing *J. Non-cryst. solids* **438** 10

[58] Grigoriev F *et al* 2017 Computational experiments on atomistic modeling of thin-film deposition *Appl. Opt.* **56** C87–90